

The two-time Leggett-Garg inequalities of a superconducting qubit interacting with thermal photons in a cavity

Hiroo Azuma^{*}

Global Research Center for Quantum Information Science,
 National Institute of Informatics,
 2-1-2 Hitotsubashi, Chiyoda-ku, Tokyo 101-8430, Japan

January 19, 2026

Abstract

In this paper, we study the two-time Leggett-Garg (LG) inequalities of a quantum optical model that appears in the Josephson-junction quantum bit (qubit) interacting with an external magnetic flux. This model is a natural extension of an exactly solvable model whose interaction between a qubit and single-mode photons is given by a product of the Pauli z operator of the qubit and a linear combination of annihilation and creation operators of the photons. By contrast, a photon's part of the interaction of our model is given by the square of the linear combination. Because our model is not solvable, we approximately investigate its time evolution up to the second-order perturbation. Our numerical calculations show that violation of the LG inequality diminishes as the temperature increases. Moreover, it exhibits power laws of the temperature, whose exponents vary depending on the coupling constant of the interaction between the qubit and photons. The violation of the LG inequality decreases and becomes less sensitive to the temperature as the coupling constant of the interaction gets larger.

1 Introduction

Several models in the field of quantum optics play essential roles in investigations of quantum information theory [1]. For example, one may examine a model in which a two-level atom inside a cavity interacts with cavity mode photons with a specific wavelength. This can be regarded as a system depicting a quantum bit (qubit) interacting with bosonic massless particles [2, 3, 4, 5]. Furthermore, assuming that the mirrors in the cavity act

^{*}Email: zuma@nii.ac.jp

as a heat bath, we can introduce the temperature for the photons. Such models are well studied to describe the dissipation and dephasing of states of the qubit interacting with an external thermal environment [6].

From a broader perspective, atoms and photons confined within the cavity constitute an open quantum system. One can investigate not only dissipation and depahsing but also decoherence for the qubit [7, 8, 9]. Moreover, by controlling the state of the photons, we can manipulate atomic states. Reference [10] proposed a method to construct the qubit using a superconducting electrical circuit based on the Jaynes-Cummings model. Dissipation and decoherence of the multiphoton quantum Rabi oscillation in ultrastrong cavity quantum electrodynamics (QED) were investigated [11]. Resilience of the quantum Rabi model in superconducting circuit QED was investigated [12]. Müller studied the interaction between the qubits and resonators by means of an analytical approach within the dispersive regime of the Rabi model [13].

For example, we can think of a cavity QED model with the following Hamiltonian as a typical one:

$$\hat{H} = (1/2)\hbar\Omega\hat{\sigma}_z + \hbar\omega\hat{a}^\dagger\hat{a} + \hbar\hat{\sigma}_z(g\hat{a}^\dagger + g^*\hat{a}), \quad (1)$$

where \hbar denotes the Planck constant, $\Omega/(2\pi)$ denotes the frequency between the excited and ground states of the two-level atom, $\omega/(2\pi)$ denotes the frequency of the photons confined in the cavity, $\hat{\sigma}_z$ denotes the Pauli z operator acting on the atom, \hat{a} and \hat{a}^\dagger denote the annihilation and creation operators of the photons, respectively, and g denotes the coupling constant. In early studies of quantum computers, the noise tolerance of qubits was investigated by employing this Hamiltonian and assuming that the initial state of the photons was in thermal equilibrium obeying the Bose-Einstein distribution [14, 15]. The Leggett-Garg (LG) inequalities of the system described by this Hamiltonian were investigated [16]. The reason why the model with this Hamiltonian is so popular is that it can be solved exactly. Furthermore, this model often remains exactly solvable even when the single-mode photons are extended to multiple modes [17].

The LG inequality is a probe that distinguishes between quantum mechanics and macroscopic local realism [18, 19]. To compute Bell's inequality, we prepare two spatially separated qubits and obtain correlation functions between their measurements. By contrast, to evaluate the LG inequality, we examine correlations of measurements at different times for a single qubit. Thus, the LG inequality can be regarded as a temporal analog of Bell's inequality. Specifically, it tests the following two assumptions that are expected to hold in classical theory: (1) macroscopic realism and (2) noninvasive measurability.

Leggett and Garg originally proposed the three-time LG inequality as a criterion for testing macroscopic local realism. In contrast, Mawby and Halliwell introduced a two-time version of the LG inequalities [20, 21, 22]. The latter are computationally more tractable, and we adopt them in this paper. In general, the three-time LG inequality requires quantum nondemolition measurements, which makes its experimental implementation difficult. By contrast, to evaluate the two-time LG inequalities, quantum nondemolition measurements are not necessary. This fact is advantageous when we perform experiments.

In this paper, we consider a system whose Hamiltonian is represented by

$$\hat{H} = (1/2)\hbar\Omega\hat{\sigma}_z + \hbar\omega\hat{a}^\dagger\hat{a} + \hbar^2\hat{\sigma}_z(g\hat{a}^\dagger + g^*\hat{a})^2, \quad (2)$$

instead of the Hamiltonian given by Eq. (1). We can implement the Hamiltonian of Eq. (2) by constructing a qubit in a circuit with two Josephson junctions in parallel. We can introduce the interaction between the qubit and photons by threading a magnetic flux through the circuit. Because we cannot rigorously solve the time evolution of the system whose Hamiltonian is given by Eq. (2), we analyze it using the second-order perturbation theory.

Utilizing these techniques, we evaluate the two-time LG inequalities of the qubit up to the second order. We introduce the temperature to the system by assuming that the initial states of the photons are in thermal equilibrium. We examine the effects of the temperature on the violations of the two-time LG inequalities. In particular, we focus on the first local minima of the violations of the LG inequalities that are smaller than zero and the times when those local minima are observed. Regarding those values as functions of the temperature, we fit them with the power functions of the temperature approximately. Our numerical calculations show that an increase in temperature causes the transition from quantum to classical behavior for the system.

This paper is organized as follows. In Sec. 2, we show how to construct the Josephson-junction qubit which interacts with thermal photons in the cavity. In Sec. 3, we introduce the two-time LG inequalities and observables. In Sec. 4, we formulate the time-evolution operator and correlation functions. In Sec. 5, we give mathematical expressions that are included in the correlation functions according to the second-order perturbation theory. In Sec. 6, we show results of numerical calculations. In Sec. 7, we provide concluding remarks. In Appendix A, we explain how to derive the mathematical expressions given in Sec. 5. In Appendix B, we show the rigorous solution of the time evolution caused by the Hamiltonian given by Eq. (1).

2 The Josephson-junction qubit interacting with the thermal photons in the cavity

In this section, we build the qubit with Josephson junctions, which are interacting with an external magnetic flux. Figure 1 shows a circuit constructed from two Josephson junctions in parallel and a magnetic field \mathbf{B} applied through the interior of the loop [23, 24, 25, 26, 27]. We denote the phase differences of a wave function between points 1 and 2 along the paths of Josephson junctions a and b as δ_a and δ_b , respectively. Moreover, denoting the external magnetic flux of the magnetic field \mathbf{B} as Φ , we have

$$\delta_a = \delta_0 - \frac{e}{\hbar c} \Phi, \quad \delta_b = \delta_0 + \frac{e}{\hbar c} \Phi, \quad (3)$$

where δ_0 is a constant. We denote a total current and currents along junctions a and b as J_{total} , J_a , and J_b , respectively. Because the Josephson effect induces J_a and J_b , we have

$$J_{\text{total}} = J_a + J_b = 2J_0 \sin \delta_0 \cos \frac{e\Phi}{\hbar c}, \quad (4)$$

where J_0 is the maximum zero-voltage current. Furthermore, because

$$J_0 \propto \hat{\sigma}_z = |\text{L}\rangle\langle\text{L}| - |\text{R}\rangle\langle\text{R}|, \quad (5)$$

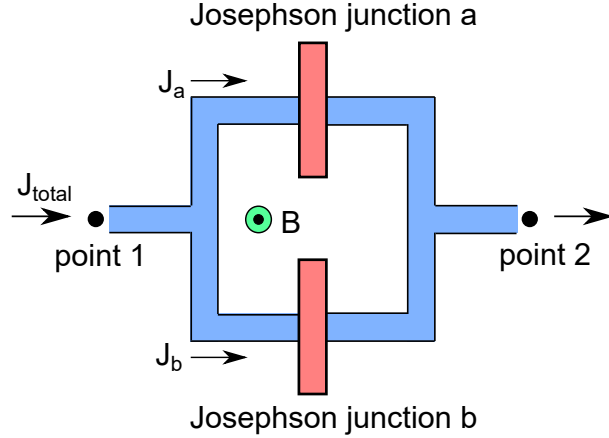


Figure 1: A circuit with two Josephson junctions in parallel. The magnetic field pierces the plane of the circuit.

where $|L\rangle$ and $|R\rangle$ are the left- and right-circulating persistent current states, respectively, and

$$\Phi \propto \hat{a} + \hat{a}^\dagger, \quad (6)$$

we obtain

$$J_{\text{total}} \propto \hat{\sigma}_z \cos(\hat{a} + \hat{a}^\dagger) = \hat{\sigma}_z + \frac{1}{2} \hat{\sigma}_z (\hat{a} + \hat{a}^\dagger)^2 + \dots \quad (7)$$

We can write Eq. (6) because $\langle \alpha | (\hat{a} + \hat{a}^\dagger) | \alpha \rangle = 2\text{Re}[\alpha]$, where the magnetic field \mathbf{B} is represented as a coherent state $|\alpha\rangle$ with phase α .

Here, we assume that the two Josephson junctions are placed in a cavity and the qubit is constructed from the two states $\{|L\rangle, |R\rangle\}$ interacting with single-mode photons. Then, a total Hamiltonian of the Josephson-junction qubit and the single photons is given by Eq. (2) where $\Omega/(2\pi)$ denotes the frequency between $|L\rangle$ and $|R\rangle$ of the Josephson-junction qubit.

From now on, we write the system of the qubit and photons as Q and P , respectively. We define eigenstates of $\hat{\sigma}_z$ as $\hat{\sigma}_z |e\rangle_Q = |e\rangle_Q$ and $\hat{\sigma}_z |g\rangle_Q = -|g\rangle_Q$. We assume that mirrors surrounding the cavity can be regarded as a heat bath whose temperature is given by $(k_B\beta)^{-1}$, where k_B denotes the Boltzmann constant. Thus, the photons obey the Bose-Einstein distribution. Accordingly, the initial state of the photons is in thermal equilibrium and given by

$$\hat{\rho}_{0,P} = (1 - e^{-\beta\omega}) \exp(-\beta\omega \hat{a}^\dagger \hat{a}), \quad (8)$$

where we put $\hbar = 1$. Defining the initial state of the Josephson-junction qubit as $\hat{\rho}_{0,Q} = |g\rangle\langle g|$, we obtain the initial state of the whole system as $\hat{\rho}_0 = \hat{\rho}_{0,Q} \otimes \hat{\rho}_{0,P}$.

3 The two-time LG inequalities and observables

In this section, we introduce the two-time LG inequalities and observables for the qubit. The two-time LG inequalities are defined as

$$\text{LG}_{s_0, s_1} = \langle (1 + s_0 \hat{A}_0)(1 + s_1 \hat{A}_1) \rangle \geq 0, \quad (9)$$

$$\langle \hat{A}_0 \rangle = \sum_{A_0 \in \{\pm 1\}} p(A_0) A_0, \quad (10)$$

$$\langle \hat{A}_1 \rangle = \sum_{A_1 \in \{\pm 1\}} p(A_1) A_1, \quad (11)$$

$$\langle \hat{A}_0 \hat{A}_1 \rangle = \sum_{A_0, A_1 \in \{\pm 1\}} p(A_0, A_1) A_0 A_1, \quad (12)$$

where $s_0, s_1 \in \{\pm 1\}$, \hat{A}_0 and \hat{A}_1 are observables of the qubit at time t_0 and t_1 , respectively, A_0 and A_1 are values of outcomes of measurements with \hat{A}_0 and \hat{A}_1 , respectively, $p(A_0, A_1)$ is a probability that A_0 and A_1 are obtained, $p(A_0) = \sum_{A_1 \in \{\pm 1\}} p(A_0, A_1)$, and $p(A_1) = \sum_{A_0 \in \{\pm 1\}} p(A_0, A_1)$. Here, we set $t_0 = 0$, that is, the initial time, and $t_1 > 0$.

Next, we define the observable of the qubit as

$$\hat{A} = a_x \hat{\sigma}_x + a_y \hat{\sigma}_y + a_z \hat{\sigma}_z = a \hat{\sigma}_+ + a^* \hat{\sigma}_- + a_z \hat{\sigma}_z, \quad (13)$$

where $\hat{\sigma}_{\pm} = (1/2)(\hat{\sigma}_x \pm i\hat{\sigma}_y)$, $a = a_x + ia_y$, and $\hat{\sigma}_x$, $\hat{\sigma}_y$, and $\hat{\sigma}_z$ are Pauli matrices acting on the qubit. Because a term which is proportional to the identity matrix $\hat{\mathbf{I}}$ only adds a constant to the outcomes of the measurements and it does not affect physics essentially, we drop $\hat{\mathbf{I}}$ in Eq. (13). Moreover, assuming that eigenvalues of \hat{A} is given by ± 1 , we obtain

$$|a_x|^2 + |a_y|^2 + |a_z|^2 = |a|^2 + |a_z|^2 = 1. \quad (14)$$

Projection operators $\{\hat{\Pi}_{\mu} : \mu = \pm 1\}$ are given by

$$\hat{\Pi}_{\mu} = (1/2)(\hat{\mathbf{I}} + \mu \hat{A}). \quad (15)$$

4 The time-evolution operator and correlation functions

In this section, we formulate a time-evolution unitary operator and correlation functions. First of all, we construct the time-evolution operator with the Hamiltonian given by Eq. (2) as

$$\begin{aligned} \hat{U}(t_1, t_0) &= \exp[-i\Omega(t_1 - t_0)/2] \exp[-i\hat{H}_+(t_1 - t_0)] |e\rangle\langle e| \\ &\quad + \exp[i\Omega(t_1 - t_0)/2] \exp[-i\hat{H}_-(t_1 - t_0)] |g\rangle\langle g|, \end{aligned} \quad (16)$$

where

$$\hat{H}_{\pm} = \omega \hat{a}^\dagger \hat{a} \pm (g \hat{a}^\dagger + g^* \hat{a})^2, \quad (17)$$

$t_1 > t_0$, and $\hat{U}(t_1, t_0)$ transform a state at time t_0 into a state at time t_1 . Here, we rewrite \hat{H}_\pm as the following convenient forms:

$$\hat{H}_\pm = \omega_\pm \hat{a}^\dagger \hat{a} \pm (\kappa \hat{a}^2 + \kappa^* \hat{a}^2) \pm |g|^2, \quad (18)$$

where $\omega_\pm = \omega \pm 2|g|^2$ and $\kappa = g^2$. Next, we compute a probability $P(\mu, t_1; \nu, t_0)$ that we observe μ and ν at time t_1 and time t_0 , respectively, where $\mu, \nu \in \{\pm 1\}$, using the projection operators $\{\hat{\Pi}_{\pm 1}\}$ defined by Eq. (15). Because it is given in the form,

$$P(\mu, t_1; \nu, t_0) = \text{Tr}[\hat{\Pi}_\nu(0)\hat{\Pi}_\mu(t_1 - t_0)\hat{\Pi}_\nu(0)\hat{\rho}_0], \quad (19)$$

where

$$\hat{\Pi}_\mu(t_1 - t_0) = \hat{U}^\dagger(t_1, t_0)\hat{\Pi}_\mu\hat{U}(t_1, t_0), \quad (20)$$

and we define

$$\begin{aligned} \hat{A}(t_1 - t_0) &= \hat{U}^\dagger(t_1, t_0)\hat{A}\hat{U}(t_1, t_0) \\ &= \exp[i\Omega(t_1 - t_0)]\hat{V}(t_1, t_0)a\hat{\sigma}_+ + \exp[-i\Omega(t_1 - t_0)]\hat{V}^\dagger(t_1, t_0)a^*\hat{\sigma}_- \\ &\quad + a_z\hat{\sigma}_z, \end{aligned} \quad (21)$$

where

$$\hat{V}(t_1, t_0) = \exp[i\hat{H}_+(t_1 - t_0)]\exp[-i\hat{H}_-(t_1 - t_0)], \quad (22)$$

we obtain

$$\begin{aligned} P(\mu, t_1; \nu, t_0) &= \frac{3}{8} + \frac{1}{4}\nu\langle\hat{A}(0)\rangle_0 + \frac{1}{8}\mu\langle\hat{A}(t_1 - t_0)\rangle_0 + \frac{1}{4}\mu\nu\text{Re}[\langle\hat{A}(t_1 - t_0)\hat{A}(0)\rangle_0] \\ &\quad + \frac{1}{8}\mu\langle\hat{A}(0)\hat{A}(t_1 - t_0)\hat{A}(0)\rangle_0, \end{aligned} \quad (23)$$

where $\langle\hat{X}\rangle_0 = \text{Tr}[\hat{X}\hat{\rho}_0]$. Here, we draw attention that $p(A_0, A_1) = P(A_1, t_1; A_0, t_0)$.

We can calculate $\langle\hat{A}_0\rangle = \langle\hat{A}(0)\rangle_0$ given by Eq. (10) with ease because $\langle\hat{A}\rangle_0 = \text{Tr}[\hat{A}(0)\hat{\rho}_{0,Q}]$. According to Eqs. (11), (12), and (23), we obtain

$$\langle\hat{A}_1\rangle = \frac{1}{2}\langle\hat{A}(t_1 - t_0)\rangle_0 + \frac{1}{2}\langle\hat{A}(0)\hat{A}(t_1 - t_0)\hat{A}(0)\rangle_0, \quad (24)$$

$$\langle\hat{A}_0\hat{A}_1\rangle = \text{Re}[\langle\hat{A}(t_1 - t_0)\hat{A}(0)\rangle_0]. \quad (25)$$

Using Eq. (21), we can rewrite $\langle\hat{A}(t_1 - t_0)\rangle_0$, $\langle\hat{A}(t_1 - t_0)\hat{A}(0)\rangle_0$, and $\langle\hat{A}(0)\hat{A}(t_1 - t_0)\hat{A}(0)\rangle_0$ as

$$\langle\hat{A}(t_1 - t_0)\rangle_0 = 2\text{Re}\{\exp[i\Omega(t_1 - t_0)]a\text{Tr}[\hat{\sigma}_+\hat{\rho}_{0,Q}]\text{Tr}[\hat{V}(t_1, t_0)\hat{\rho}_{0,P}]\} + a_z\text{Tr}[\hat{\sigma}_z\hat{\rho}_{0,Q}], \quad (26)$$

$$\begin{aligned} \langle\hat{A}(t_1 - t_0)\hat{A}(0)\rangle_0 &= 2\text{Re}\{\exp[i\Omega(t_1 - t_0)]a\text{Tr}[\hat{\sigma}_+\hat{A}(0)\hat{\rho}_{0,Q}]\text{Tr}[\hat{V}(t_1, t_0)\hat{\rho}_{0,P}]\} \\ &\quad + a_z\text{Tr}[\hat{\sigma}_z\hat{A}(0)\hat{\rho}_{0,Q}], \end{aligned} \quad (27)$$

$$\begin{aligned} \langle\hat{A}(0)\hat{A}(t_1 - t_0)\hat{A}(0)\rangle_0 &= 2\text{Re}\{\exp[i\Omega(t_1 - t_0)]a\text{Tr}[\hat{A}(0)\hat{\sigma}_+\hat{A}(0)\hat{\rho}_{0,Q}]\text{Tr}[\hat{V}(t_1, t_0)\hat{\rho}_{0,P}]\} \\ &\quad + a_z\text{Tr}[\hat{A}(0)\hat{\sigma}_z\hat{A}(0)\hat{\rho}_{0,Q}]. \end{aligned} \quad (28)$$

Because of Eqs. (26), (27), and (28), we understand that what we must do is computing $\text{Tr}[\hat{V}(t_1, t_0)\hat{\rho}_{0,P}]$.

5 Evaluation of $\text{Tr}[\hat{V}(t_1, t_0)\hat{\rho}_{0,P}]$

As explained in Appendix A, $\text{Tr}[\hat{V}(t_1, t_0)\hat{\rho}_{0,P}]$ is given in the form,

$$\text{Tr}[\hat{V}(t_1, t_0)\hat{\rho}_{0,P}] = (1 - e^{-\beta\omega}) \sum_{m=0}^{\infty} \exp(-m\beta\omega) \mathcal{F}(m), \quad (29)$$

where

$$\begin{aligned} \mathcal{F}(m) = & F(m) \left\{ 1 - \frac{1}{2} |\tilde{\kappa}_+|^2 [\theta(m-2)m(m-1) + (m+1)(m+2)] \right\} \\ & \times \left\{ 1 - \frac{1}{2} |\tilde{\kappa}_-|^2 [\theta(m-2)m(m-1) + (m+1)(m+2)] \right\} \\ & - F(m+2)\tilde{\kappa}_+^*\tilde{\kappa}_-(m+1)(m+2) - F(m-2)\tilde{\kappa}_-^*\tilde{\kappa}_+\theta(m-2)m(m-1) \\ & + \frac{1}{4} F(m+4)\tilde{\kappa}_+^{*2}\tilde{\kappa}_-^2(m+1)(m+2)(m+3)(m+4) \\ & + \frac{1}{4} F(m-4)\tilde{\kappa}_-^{*2}\tilde{\kappa}_+^2\theta(m-4)m(m-1)(m-2)(m-3), \end{aligned} \quad (30)$$

$$\begin{aligned} F(n) = & \exp \left[iT^2 |\kappa|^2 \frac{\tilde{T}_+ - \sin \tilde{T}_+}{\tilde{T}_+} f(n) \right] e^{iH_0^{(+)} T} e^{-iH_0^{(-)} T} \\ & \times \exp \left[-iT^2 |\kappa|^2 \frac{\tilde{T}_- - \sin \tilde{T}_-}{\tilde{T}_-} f(n) \right] + O(|\kappa|^3), \end{aligned} \quad (31)$$

$$\tilde{\kappa}_\pm = \frac{T}{\tilde{T}_\pm} (e^{i\tilde{T}_\pm} - 1) \kappa, \quad (32)$$

$$\theta(m) = \begin{cases} 1 & m \geq 0 \\ 0 & m < 0 \end{cases}, \quad (33)$$

$\tilde{T}_\pm = 2T\omega_\pm$, $T = t_1 - t_0$, $H_0^{(\pm)} = \omega_\pm n \pm |g|^2$, and $f(n) = -2(1 + 2n)$. Here, we draw attention to the fact that $T = t_1 - t_0$ is different from the temperature $(k_B\beta)^{-1}$. Furthermore, $\tilde{\kappa}_\pm$ and \tilde{T}_\pm are dimensionless quantities.

6 Numerical calculations

In Fig. 2, we plot LG_{s_0, s_1} for $s_0, s_1 \in \{\pm 1\}$ given by Eq. (9) as functions of time $T = t_1 - t_0 (\geq 0)$. Looking at Figs. 2(a), (b), (c), and (d), we note that only $\text{LG}_{1,-1}$ violates the two-time LG inequality. Comparing the curves of $\beta = 10, 1.5$, and 0.8 in Fig. 2(b), the first local minimum value of $\text{LG}_{1,-1}$ from the time $T = 0$ becomes larger as the temperature increases. Simultaneously, the time when $\text{LG}_{1,-1}$ takes the first local minimum value approaches zero as the temperature increases. Hence, we concentrate on calculating $\text{LG}_{1,-1}$.

In Fig. 3, we plot $-\text{LG}_{\min}$ and T_{\min} as functions of the temperature β^{-1} , where LG_{\min} represents the first local minimum value of $\text{LG}_{1,-1}$ from $T = 0$ and T_{\min} represents the

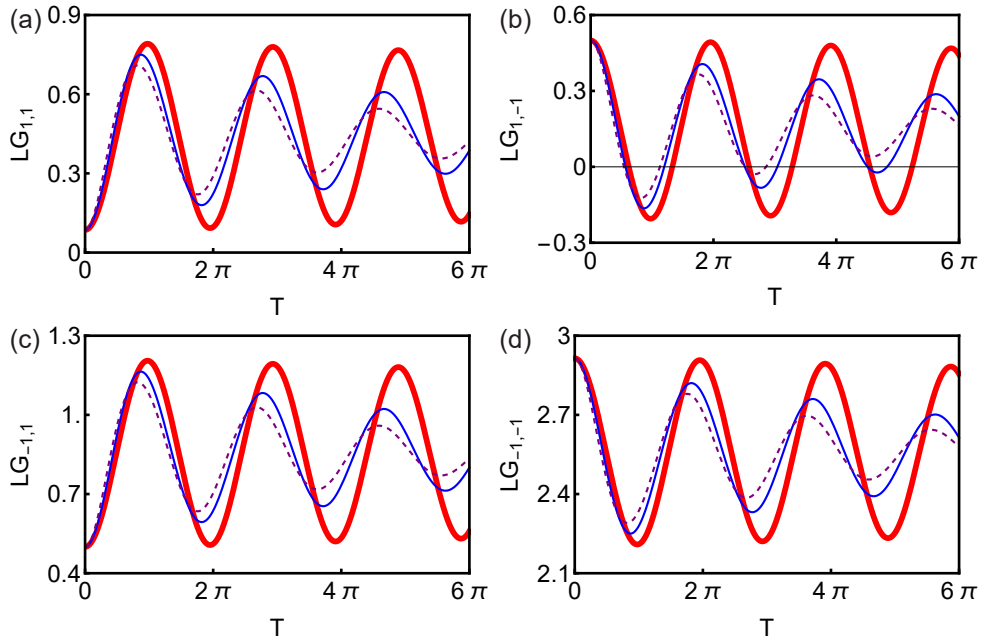


Figure 2: Plots of LG_{s_0, s_1} for $s_0, s_1 \in \{\pm 1\}$ as functions of $T = t_1 - t_0 (\geq 0)$. Curves of (a), (b), (c), and (d) represent $LG_{1,1}$, $LG_{1,-1}$, $LG_{-1,1}$, and $LG_{-1,-1}$, respectively. In those plots, we set $\Omega = 1$, $g = 0.075$, $\omega = 0.1$, $a_x = a_z = 1/\sqrt{2}$, and $a_y = 0$. The thick solid red, thin solid blue, and thin dashed purple curves represent $\beta = 10, 1.5$, and 0.8 , respectively, for (a), (b), (c), and (d). Looking at (b), we note that $LG_{1,-1} < 0$ at specific times, so that violation of the two-time LG inequality occurs at those times.

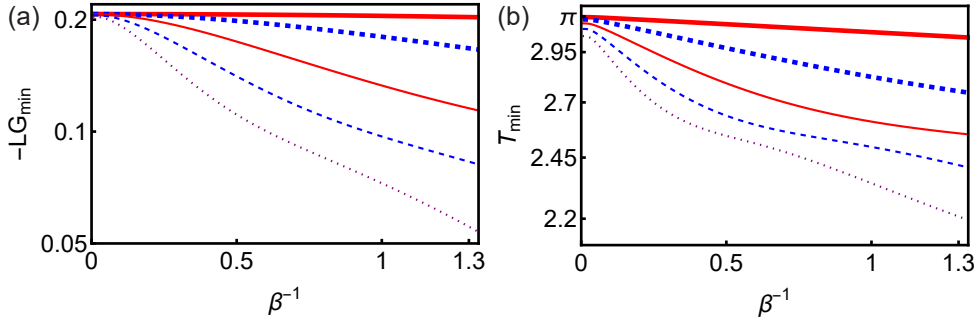


Figure 3: (a) Plots of $-\text{LG}_{\min}$ as a function of the temperature β^{-1} , where LG_{\min} represents the first local minimum value of $\text{LG}_{1,-1}$ as a function of the time $T = t_1 - t_0 (\geq 0)$. (b) Plots of T_{\min} as a function of the temperature β^{-1} , where T_{\min} represents the time when $\text{LG}_{1,-1}$ takes the first local minimum value LG_{\min} . The thick solid red, thick dashed blue, thin solid red, thin dashed blue, and thin dotted purple curves represent $g = 0.26, 0.52, 0.78, 1.04$, and 1.3 , respectively. The other parameters are set as $\Omega = 1$, $\omega = 0.1$, $a_x = a_z = 1/\sqrt{2}$, and $a_y = 0$. In graphs (a) and (b), the vertical axis is shown on a logarithmic scale.

time when $\text{LG}_{1,-1}$ take the value LG_{\min} . As the temperature increases, $-\text{LG}_{\min}$ and T_{\min} get smaller. This implies that the violation of the two-time LG inequality diminishes and the activity of the system is gradually governed by classical physics as the temperature increases. At the same time, the violation of the two-time LG inequality is reduced as the coupling constant g gets larger. We can interpret this fact as follows. As the coupling constant of the interaction between the qubit and photons in the cavity increases, the effect of the heat bath on the qubit via the cavity photons enlarges. Thus, the increase of g lets the violation of the LG inequality decrease.

In Figs. 4(a) and (b), we perform curve fitting to the data of $\{(\beta^{-1}, \log(-\text{LG}_{\min}))\}$ and $\{(\beta^{-1}, \log T_{\min})\}$ using the approximate functions,

$$\log(-\text{LG}_{\min}) = a_1 \beta^{-b_1} + c_1, \quad (34)$$

and

$$\log T_{\min} = a_2 \beta^{-b_2} + c_2, \quad (35)$$

respectively. Looking at Figs. 4(a) and (b), we note that the curve fittings are reliable for $g = 0.52$ but unreliable for $g = 1.04$. Thus, we apply these curve fittings to the data for $0 < g \leq 0.52$.

In Figs. 5(a) and (b), we plot the constants b_1 and b_2 as functions of g , respectively. Figure 5(a) shows that b_1 decreases as g gets larger. Figure 5(b) shows that b_2 has a local maximum at $g = 0.0234$. Because we fit the data using the functions given by Eqs. (34) and (35), $-\text{LG}_{\min}$ and T_{\min} becomes more sensitive to the change of the temperature if b_1 and b_2 gets larger. The exponent b_1 monotonically decreases as the coupling constant g gets larger. Although the exponent b_2 takes the local maximum at $g = 0.0234$, it monotonically decreases as g gets larger for $g > 0.0234$. Hence, the $\text{LG}_{1,-1}$ becomes less sensitive to the temperature as g gets larger. We note that the increase in the coupling

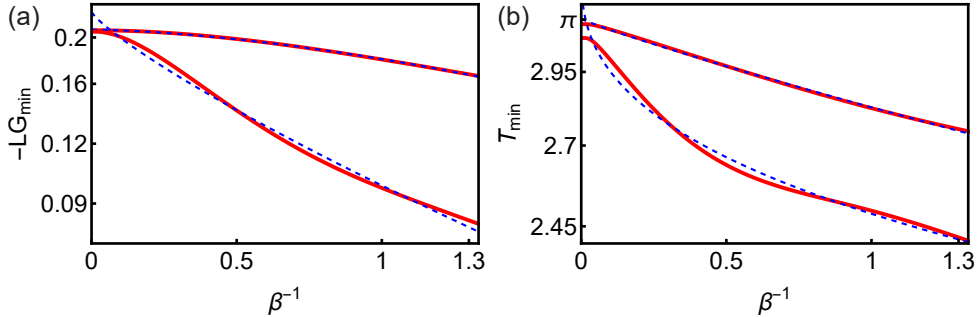


Figure 4: (a) The solid red curves represent plots of $-\text{LG}_{\min}$ as functions of the temperature β^{-1} . The dashed blue curves represent the results of fitting approximate functions $a_1\beta^{-b_1} + c_1$ to $\log(-\text{LG}_{\min})$. (b) The solid red curves represent plots of T_{\min} as functions of the temperature β^{-1} . The dashed blue curves represent the results of fitting approximate functions $a_2\beta^{-b_2} + c_2$ to $\log T_{\min}$. For both graphs (a) and (b), the upper solid red and dashed blue curves correspond to the case of $g = 0.52$, while the lower solid red and dashed blue curves correspond to the case of $g = 1.04$. In the graphs, the vertical axis is shown on a logarithmic scale.

constant g makes the violation of the LG inequality smaller in Fig. 3. At the same time, the sensitivity of the violation to temperature is reduced as g increases.

Finally, we compare the LG inequalities of the Hamiltonian given by Eq. (2) with those of the Hamiltonian given by Eq. (1). In the system governed by the Hamiltonian of Eq. (1), $\text{LG}_{1,-1}$ violates the LG inequality but $\text{LG}_{1,1}$, $\text{LG}_{-1,1}$, and $\text{LG}_{-1,-1}$ obey the LG inequalities as in the cases for the system whose Hamiltonian is given by Eq. (2). In Fig. 6, we plot $\text{LG}_{1,-1}$ as a function of the time T for the inverses of temperature $\beta = \infty, 8, 4$, and 1.5 . Looking at Fig. 6, we note that the curve of $\beta = 1.5$ does not violate the LG inequality. By contrast, Fig. 2(b) shows that the curve of $\beta = 1.5$ violates the LG inequality. Thus, we conclude that the system whose Hamiltonian is given by Eq. (1) is less robust than that with the Hamiltonian of Eq. (2) from the viewpoint of quantumness.

7 Concluding remarks

In this paper, we derived a quantum optical model implemented with a superconducting Josephson-junction circuit and investigated its time evolution with initial states of the photons in the thermal equilibrium. Because we were not able to solve this model exactly, we used the second-order perturbation theory. Calculating correlation functions, we evaluated the two-time LG inequalities and found their violations. By calculating the first local minimum values of the LG inequality that were smaller than zero and the times when those values were observed, we plotted them as functions of the temperature, fitted them using power functions of the temperature, and obtained their exponents. Our numerical estimations showed that the violation of the LG inequality decreases as the temperature increases. Moreover, the violation of the LG inequality becomes smaller and

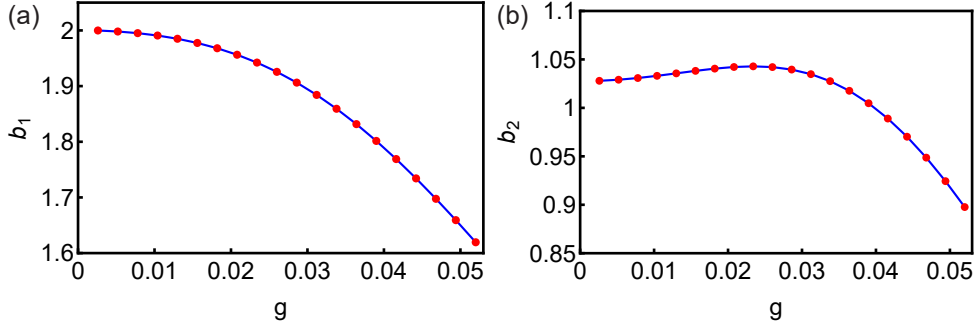


Figure 5: (a) A plot of the constant b_1 as a function of g , where b_1 is obtained by the fitting of $\{(\beta^{-1}, \log(-LG_{\min}))\}$ with the approximate function $a_1\beta^{-b_1} + c_1$. (b) A plot of the constant b_2 as a function of g , where b_2 is obtained by the fitting of $\{(\beta^{-1}, \log T_{\min})\}$ with the approximate function $a_2\beta^{-b_2} + c_2$. In both graphs (a) and (b), the red points represent the data obtained from the fitting. We join those points with blue curves.

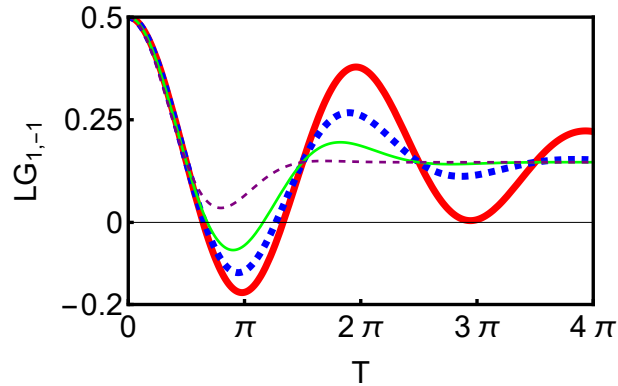


Figure 6: Plots of $LG_{1,-1}$ of the system whose Hamiltonian is given by Eq. (1) as functions of the time T . The thick solid red, thick dashed blue, thin solid green, and thin dashed purple curves represent $\beta = \infty, 8, 4$, and 1.5 , respectively. In those plots, we set $\Omega = 1$, $g = 0.075$, $\omega = 0.1$, $a_x = a_z = 1/\sqrt{2}$, and $a_y = 0$. Looking at the thick solid red curve, that is, the zero-temperature case, we note that the first local minimum at $T = \pi$ violates the LG inequality but the second local minimum at $T = 3\pi$ does not violate it.

less sensitive to temperature as the coupling constant increases.

A variety of quantum optical models have been proposed to study quantum information processing, including the multiphoton Jaynes-Cummings model [26, 27, 28, 29]. Further progress in quantum information processing is expected along this line.

Acknowledgment

This work was supported by the MEXT Quantum Leap Flagship Program Grant No. JPMXS0120351339.

A Derivation of $\text{Tr}[\hat{V}(t_1, t_0)\hat{\rho}_{0,P}]$

In this section, we compute $\text{Tr}[\hat{V}(t_1, t_0)\hat{\rho}_{0,P}]$ defined in Sec. 4 with the second-order perturbation theory. Because of Eq. (22), what we must do is to evaluate $\exp[i\hat{H}_+(t_1 - t_0)]\exp[-i\hat{H}_-(t_1 - t_0)]$. Defining $\hat{H}_\pm = \hat{H}_0^{(\pm)} \pm \hat{V}$, $\hat{H}_0^{(\pm)} = \omega_\pm \hat{a}^\dagger \hat{a} \pm |g|^2$, $\hat{V} = \kappa \hat{a}^{\dagger 2} + \kappa^* \hat{a}^2$, and $\Delta t = T/N$, we can decompose $\exp[i\hat{H}_+(t_1 - t_0)] = \exp(i\hat{H}_+T)$ by the Lie-Trotter product formula as follows:

$$\begin{aligned} \exp(i\hat{H}_+T) &= \lim_{N \rightarrow \infty} (e^{i\hat{H}_0^{(+)}\Delta t} e^{i\hat{V}\Delta t})^N \\ &= \lim_{N \rightarrow \infty} (e^{i\hat{H}_0^{(+)}\Delta t} e^{i\hat{V}\Delta t} e^{-i\hat{H}_0^{(+)}\Delta t}) (e^{2i\hat{H}_0^{(+)}\Delta t} e^{i\hat{V}\Delta t} e^{-2i\hat{H}_0^{(+)}\Delta t}) \\ &\quad \times \cdots \times (e^{Ni\hat{H}_0^{(+)}\Delta t} e^{i\hat{V}\Delta t} e^{-Ni\hat{H}_0^{(+)}\Delta t}) e^{Ni\hat{H}_0^{(+)}\Delta t} \\ &= \lim_{N \rightarrow \infty} \exp[i\Delta t(e^{2i\Delta t\omega_+} \kappa \hat{a}^{\dagger 2} + e^{-2i\Delta t\omega_+} \kappa^* \hat{a}^2)] \\ &\quad \times \exp[i\Delta t(e^{4i\Delta t\omega_+} \kappa \hat{a}^{\dagger 2} + e^{-4i\Delta t\omega_+} \kappa^* \hat{a}^2)] \\ &\quad \times \cdots \times \exp[i\Delta t(e^{2Ni\Delta t\omega_+} \kappa \hat{a}^{\dagger 2} + e^{-2Ni\Delta t\omega_+} \kappa^* \hat{a}^2)] e^{i\hat{H}_0^{(+)}T}. \end{aligned} \quad (36)$$

Here, we evaluate $e^{\hat{A}}e^{\hat{B}}$, where

$$\begin{aligned} \hat{A} &= i\Delta t(c\hat{a}^{\dagger 2} + c^* \hat{a}^2), \\ \hat{B} &= i\Delta t(c'\hat{a}^{\dagger 2} + c'^* \hat{a}^2), \end{aligned} \quad (37)$$

$c = e^{2i\Delta t\omega_+} \kappa$, and $c' = e^{4i\Delta t\omega_+} \kappa$, using the Baker-Campbell-Hausdorff formula,

$$e^{\hat{A}}e^{\hat{B}} = \exp[\hat{A} + \hat{B} + \frac{1}{2}[\hat{A}, \hat{B}] + \frac{1}{12}[\hat{A} - \hat{B}, [\hat{A}, \hat{B}]] + \cdots]. \quad (38)$$

Accordingly, we obtain

$$e^{\hat{A}}e^{\hat{B}} = \exp[\hat{A} + \hat{B} + i(\Delta t)^2 \sin(2\Delta t\omega_+) |\kappa|^2 f(\hat{n}) + O(|\kappa|^3)], \quad (39)$$

where $f(\hat{n}) = [\hat{a}^{\dagger 2}, \hat{a}^2] = -2(1 + 2\hat{n})$ and $\hat{n} = \hat{a}^\dagger \hat{a}$. To obtain $e^{i\hat{H}_+T}$ given by Eq. (36) up to the second order of κ , we must compute a term on the order of $(\Delta t)^2$ that appears in the exponent. If we define

$$\hat{C} = i\Delta t(c''\hat{a}^{\dagger 2} + c''^* \hat{a}^2), \quad (40)$$

where $c'' = e^{6i\Delta t\omega_+} \kappa$, we obtain

$$[\hat{A} + \hat{B}, \hat{C}] = 2i(\Delta t)^2 [\sin(2\Delta t\omega_+) + \sin(4\Delta t\omega_+)] |\kappa|^2 f(\hat{n}). \quad (41)$$

Hence, the term on the order of $(\Delta t)^2$ that appears in the exponent of $e^{i\hat{H}_+ T}$ is given by

$$2i(\Delta t)^2 |\kappa|^2 f(\hat{n}) \{(N-1) \sin(2\Delta t\omega_+) + (N-2) \sin(4\Delta t\omega_+) + \dots + \sin[2(N-1)\Delta t\omega_+] \}. \quad (42)$$

Because

$$\lim_{N \rightarrow \infty} \frac{1}{N^2} \sum_{k=1}^{N-1} (N-k) \sin(k\epsilon_+) = \frac{\tilde{T}_+ - \sin \tilde{T}_+}{\tilde{T}_+}, \quad (43)$$

and

$$\lim_{N \rightarrow \infty} \frac{1}{N} \sum_{k=1}^N e^{\pm ik\epsilon_+} = \mp \frac{i}{\tilde{T}_+} (e^{\pm i\tilde{T}_+} - 1), \quad (44)$$

where $\epsilon_+ = 2\Delta t\omega_+$ and $\tilde{T}_+ = N\epsilon_+ = 2T\omega_+$, we attain

$$\begin{aligned} e^{i\hat{H}_+ T} &= \exp \left[\frac{T}{\tilde{T}_+} (e^{i\tilde{T}_+} - 1) \kappa \hat{a}^{\dagger 2} - \frac{T}{\tilde{T}_+} (e^{-i\tilde{T}_+} - 1) \kappa^* \hat{a}^2 \right] \\ &\quad \times \exp \left[iT^2 |\kappa|^2 \frac{\tilde{T}_+ - \sin \tilde{T}_+}{\tilde{T}_+} f(\hat{n}) \right] e^{i\hat{H}_0^{(+)} T} + O(|\kappa|^3). \end{aligned} \quad (45)$$

In the same way as above, we obtain

$$\begin{aligned} e^{-i\hat{H}_- T} &= e^{-i\hat{H}_0^{(-)} T} \exp \left[-iT^2 |\kappa|^2 \frac{\tilde{T}_- - \sin \tilde{T}_-}{\tilde{T}_-} f(\hat{n}) \right] \\ &\quad \times \exp \left[\frac{T}{\tilde{T}_-} (e^{i\tilde{T}_-} - 1) \kappa \hat{a}^{\dagger 2} - \frac{T}{\tilde{T}_-} (e^{-i\tilde{T}_-} - 1) \kappa^* \hat{a}^2 \right] + O(|\kappa|^3). \end{aligned} \quad (46)$$

Next, we calculate a matrix element

$${}_P \langle m | \hat{V}(t_1, t_0) | m \rangle_P = {}_P \langle m | \exp(\tilde{\kappa}_+ \hat{a}^{\dagger 2} - \tilde{\kappa}_+^* \hat{a}^2) F(\hat{n}) \exp(\tilde{\kappa}_- \hat{a}^{\dagger 2} - \tilde{\kappa}_-^* \hat{a}^2) | m \rangle_P, \quad (47)$$

where $\tilde{\kappa}_\pm$ are given by Eq. (32) and

$$\begin{aligned} F(\hat{n}) &= \exp \left[iT^2 |\kappa|^2 \frac{\tilde{T}_+ - \sin \tilde{T}_+}{\tilde{T}_+} f(\hat{n}) \right] e^{i\hat{H}_0^{(+)} T} e^{-i\hat{H}_0^{(-)} T} \\ &\quad \times \exp \left[-iT^2 |\kappa|^2 \frac{\tilde{T}_- - \sin \tilde{T}_-}{\tilde{T}_-} f(\hat{n}) \right]. \end{aligned} \quad (48)$$

Thus, we obtain

$${}_P \langle m | \hat{V}(t_1, t_0) | m \rangle_P = \mathcal{F}(m) + O(|\kappa|^3), \quad (49)$$

where $\mathcal{F}(m)$ is given by Eq. (30).

B The exact solution of the time evolution with the Hamiltonian given by Eq. (1)

In this section, we derive the exact solution of the time evolution of the system whose Hamiltonian is given by Eq. (1). By the method explained in Appendix A, we can derive

$$\begin{aligned}\hat{V}'(t_1, t_0) &= e^{i\hat{H}'_+(t_1-t_0)}e^{-i\hat{H}'_-(t_1-t_0)} \\ &= \exp[2(\tilde{g}\hat{a}^\dagger - \tilde{g}^*\hat{a})] \\ &= e^{2|\tilde{g}|^2} \exp(-2\tilde{g}^*\hat{a}) \exp(2\tilde{g}\hat{a}^\dagger),\end{aligned}\quad (50)$$

where

$$\hat{H}'_\pm = \omega\hat{a}^\dagger\hat{a} \pm (g\hat{a}^\dagger + g^*\hat{a}), \quad (51)$$

$$\tilde{g} = \frac{T}{\tilde{T}}(e^{i\tilde{T}} - 1)g, \quad (52)$$

$\tilde{T} = T\omega$, and $T = t_1 - t_0$. Then, a matrix element is given by

$$\begin{aligned}_P\langle m|\hat{V}'(t_1, t_0)|m\rangle_P &= e^{2|\tilde{g}|^2} \sum_{k=0}^{\infty} {}_P\langle m|\frac{1}{(k!)^2}(-4|\tilde{g}|^2)^k\hat{a}^k\hat{a}^{+k}|m\rangle_P \\ &= e^{2|\tilde{g}|^2} \sum_{k=0}^{\infty} \frac{1}{(k!)^2}(-4|\tilde{g}|^2)^k \frac{(m+k)!}{m!} \\ &= e^{2|\tilde{g}|^2} {}_1F_1(1+m; 1; -4|\tilde{g}|^2),\end{aligned}\quad (53)$$

where ${}_1F_1(a; b; z)$ is the Kummer confluent hypergeometric function. Substituting the matrix element for $\mathcal{F}(m)$ in Eq. (29), we obtain $\text{Tr}[\hat{V}'(t_1, t_0)\hat{\rho}_{0,P}]$. Then, replacing $\text{Tr}[\hat{V}(t_1, t_0)\hat{\rho}_{0,P}]$ with $\text{Tr}[\hat{V}'(t_1, t_0)\hat{\rho}_{0,P}]$ in Eq. (26), (27), and (28), we can derive $\text{LG}_{1,-1}$ for the system whose Hamiltonian is given by Eq. (1). In particular, for the zero-temperature case, that is, $\beta = +\infty$, we obtain

$$\text{LG}_{1,-1} = \frac{1}{4} \left\{ 2 - \sqrt{2} + \sqrt{2} \cos(T\Omega) \exp\left[\frac{4g^2(-1 + \cos(T\omega))}{\omega^2}\right] \right\}. \quad (54)$$

References

- [1] M. M. Alqahtani, M. S. Everitt and B. M. Garraway, ‘Cavity QED photons for quantum information processing’, *J. Phys. B: At. Mol. Opt. Phys.* **55**, 184004 (2022).
doi: 10.1088/1361-6455/ac864f
- [2] J. M. Raimond, M. Brune, and S. Haroche, ‘Manipulating quantum entanglement with atoms and photons in a cavity’, *Rev. Mod. Phys.* **73**, 565–582 (2001).
doi: 10.1103/RevModPhys.73.565
- [3] F. Beaudoin, J. M. Gambetta, and A. Blais, ‘Dissipation and ultrastrong coupling in circuit QED’, *Phys. Rev. A* **84**, 043832 (2011).
doi: 10.1103/PhysRevA.84.043832

- [4] N. Meher and S. Sivakumar, ‘A review on quantum information processing in cavities’, *Eur. Phys. J. Plus* **137**, 985 (2022).
`doi: 10.1140/epjp/s13360-022-03172-x`
- [5] Q. Bin, Y. Wu, J.-H. Gao, A. Chen, F. Nori, and X.-Y. Lü, ‘Cavity QED based on strongly localized modes: exponentially enhancing single-atom cooperativity’, *Phys. Rev. Lett.* **135**, 103602 (2025).
`doi: 10.1103/7frd-pf1m`
- [6] M. Ban, ‘Decoherence of a two-level system in a coherent superposition of two dephasing environments’, *Quantum Inf. Process.* **19**, 409 (2020).
`doi: 10.1007/s11128-020-02903-2`
- [7] Q.-L. He, J.-B. Xu, D.-X. Yao, and Y.-Q. Zhang, ‘Sudden transition between classical and quantum decoherence in dissipative cavity QED and stationary quantum discord’, *Phys. Rev. A* **84**, 022312 (2011).
`doi: 10.1103/PhysRevA.84.022312`
- [8] P. Kaer and J. Mørk, ‘Decoherence in semiconductor cavity QED systems due to phonon couplings’, *Phys. Rev. B* **90**, 035312 (2014).
`doi: 10.1103/PhysRevB.90.035312`
- [9] J. Dajka, ‘Pure decoherence of the Jaynes-Cummings model: initial entanglement with the environment, spin oscillations and detection of non-orthogonal states’, *Symmetry* **16**, 250 (2024).
`doi: 10.3390/sym16020250`
- [10] A. Blais, R.-S. Huang, A. Wallraff, S. M. Girvin, and R. J. Schoelkopf, ‘Cavity quantum electrodynamics for superconducting electrical circuits: An architecture for quantum computation’, *Phys. Rev. A* **69**, 062320 (2004).
`doi: 10.1103/PhysRevA.69.062320`
- [11] L. Garziano, R. Stassi, V. Macrì, A. F. Kockum, S. Savasta, and F. Nori, ‘Multiphoton quantum Rabi oscillations in ultrastrong cavity QED’, *Phys. Rev. A* **92**, 063830 (2015).
`doi: 10.1103/PhysRevA.92.063830`
- [12] V. E. Manucharyan, A. Baksic, and C. Ciuti, ‘Resilience of the quantum Rabi model in circuit QED’, *J. Phys. A: Math. Theor.* **50** 294001 (2017).
`doi: 10.1088/1751-8121/aa6fbc`
- [13] C. Müller, ‘Dissipative Rabi model in the dispersive regime’, *Phys. Rev. Research* **2**, 033046 (2020).
`doi: 10.1103/PhysRevResearch.2.033046`
- [14] G. M. Palma, K.-A. Suominen, and A. K. Ekert, ‘Quantum computers and dissipation’, *Proc. R. Soc. Lond. A* **452**, 567–584 (1996).
`doi: 10.1098/rspa.1996.0029`

- [15] J. H. Reina, L. Quiroga, and N. F. Johnson, ‘Decoherence of quantum registers’, *Phys. Rev. A* **65**, 032326 (2002).
doi: [10.1103/PhysRevA.65.032326](https://doi.org/10.1103/PhysRevA.65.032326)
- [16] R. Usui and M. Ban, ‘Temporal nonlocality of a two-level system interacting with a dephasing environment’, *Quantum Inf. Process.* **19**, 159 (2020).
doi: [10.1007/s11128-020-02656-y](https://doi.org/10.1007/s11128-020-02656-y)
- [17] A. J. Leggett, S. Chakravarty, A. T. Dorsey, M. P. A. Fisher, A. Garg, and W. Zwerger, ‘Dynamics of the dissipative two-state system’, *Rev. Mod. Phys.* **59**, 1–85 (1987); *Rev. Mod. Phys.* **67**, 725–726 (1995).
doi: [10.1103/RevModPhys.59.1](https://doi.org/10.1103/RevModPhys.59.1)
doi: [10.1103/RevModPhys.67.725](https://doi.org/10.1103/RevModPhys.67.725)
- [18] A. J. Leggett and A. Garg, ‘Quantum mechanics versus macroscopic realism: Is the flux there when nobody looks?’, *Phys. Rev. Lett.* **54**, 857–860 (1985).
doi: [10.1103/PhysRevLett.54.857](https://doi.org/10.1103/PhysRevLett.54.857)
- [19] C. Emery, N. Lambert, and F. Nori, ‘Leggett-Garg inequalities’, *Rep. Prog. Phys.* **77** 016001 (2014).
doi: [10.1088/0034-4885/77/1/016001](https://doi.org/10.1088/0034-4885/77/1/016001)
- [20] J. J. Halliwell, ‘Comparing conditions for macrorealism: Leggett-Garg inequalities versus no-signaling in time’, *Phys. Rev. A* **96**, 012121 (2017).
doi: [10.1103/PhysRevA.96.012121](https://doi.org/10.1103/PhysRevA.96.012121)
- [21] J. J. Halliwell and C. Mawby, ‘Fine’s theorem for Leggett-Garg tests with an arbitrary number of measurement times’, *Phys. Rev. A* **100**, 042103 (2019).
doi: [10.1103/PhysRevA.100.042103](https://doi.org/10.1103/PhysRevA.100.042103)
- [22] C. Mawby and J. J. Halliwell, ‘Leggett-Garg violations for continuous-variable systems with Gaussian states’, *Phys. Rev. A* **107**, 032216 (2023).
doi: [10.1103/PhysRevA.107.032216](https://doi.org/10.1103/PhysRevA.107.032216)
- [23] C. Kittel, *Introduction to Solid State Physics*, 7th ed. (Wiley, New York, 1996).
- [24] R. P. Feynman, R. B. Leighton, and M. Sands, *The Feynman Lectures on Physics: Quantum Mechanics, The Definitive Edition* (Addison-Wesley, Reading, 2006), Vol. III.
- [25] S. Felicetti, D. Z. Rossatto, E. Rico, E. Solano, and P. Forn-Díaz, ‘Two-photon quantum Rabi model with superconducting circuits’, *Phys. Rev. A* **97**, 013851 (2018).
doi: [10.1103/PhysRevA.97.013851](https://doi.org/10.1103/PhysRevA.97.013851)
- [26] H. Azuma, ‘Quasiperiodic trajectories drawn by the Bloch vector of the thermal multiphoton Jaynes-Cummings model’, *Int. J. of Theor. Phys.* **64**, 153 (2025).
doi: [10.1007/s10773-025-06017-2](https://doi.org/10.1007/s10773-025-06017-2)

- [27] H. Azuma, W. J. Munro, and K. Nemoto, ‘Quantum phase transitions in the multi-photon Jaynes-Cummings-Hubbard model’, *Phys. Rev. A* **112**, 033709 (2025).
doi: [10.1103/ypts-6z4p](https://doi.org/10.1103/ypts-6z4p)
- [28] J. Tang, ‘Quantum switching between nonclassical correlated single photons and two-photon bundles in a two-photon Jaynes-Cummings model’, *Opt. Express* **31**, 12471–12486 (2023).
doi: [10.1364/OE.487297](https://doi.org/10.1364/OE.487297)
- [29] H. Azuma, ‘Insensitivity of the two-photon Jaynes-Cummings model to thermal noise’, *Phys. Rev. A* **110**, 063714 (2024).
doi: [10.1103/PhysRevA.110.063714](https://doi.org/10.1103/PhysRevA.110.063714)